Supplementary Information (SI) for Energy & Environmental Science.
This journal is © The Royal Society of Chemistry 2024

Supporting Information

Suppressing Product Crossover and C-C Bond Cleavage in a Glycerol Membrane Electrode Assembly Reformer

Chencheng Dai, Qian Wu, Tianze Wu, Yuwei Zhang, Libo Sun, Xin Wang, Adrian C. Fisher, Zhichuan J. Xu*

Experimental Details

Materials

The Toray 090 carbon paper, FAA-3 ionomer solution, Nafion D-520 solution and Nafion 212 proton exchange membrane (PEM) were purchased from Fuel Cell Store, US. The Ni fiber paper and Sustainion X37-50 Grade T anion exchange membrane (AEM) were purchased from Dioxide Materials, US. The 40 wt% Pt on high surface area Ketjenblack and 40 wt% Pt on Vulcan Carbon were purchased from Premetek, US. The SS316l bipolar plates were fabricated by Axis Synergy, Singapore, and the Ti bipolar plates were fabricated by Baoji Yinggao, China. All other chemicals were purchased from Sigma Aldrich and used without purification. Deionized water with resistance of 18.2 MΩ cm was used for all experiments.

Electrochemical tests in H-cell

The electrochemical glycerol oxidation coupling with hydrogen evolution reaction was first tested in an H-cell with two chambers separated by an alkaline-pretreated Nafion 212 membrane (The membrane was immersed in the 1 M KOH solution overnight before the test.). The two-electrode setup employed a glassy carbon electrode (5 mm diameter) drop cast with 1 mg_{pt} cm^{-2} 40 wt% Pt/Ketjenblack (from catalyst ink of 5 mg ml^{-1} 40 wt% Pt/Ketjenblack in IPA : deionized water : 5 wt% Nafion ionomer solution = 4 : 1 : 0.0486, to form 10 wt% Nafion ionomer in the catalyst layer) and a Pt plate (2 cm * 2 cm) as the working and counter electrode, respectively. The three-electrode setup employed an additional Hg/HgO (1 M KOH) reference electrode. The anode and cathode chambers both with alkaline electrolyte were tested with both three-electrode and two-electrode systems (1 & 2 M KOH with 0.5 & 1 M glycerol anolyte, 1 & 2 M KOH catholyte) to measure both the catalyst activity and whole cell voltage. The alkaline anolyte (1 & 2 M KOH with 0.5 & 1 M glycerol) and acidic catholyte (0.5 & 1 M H_2SO_4) tests were only measured by the two-electrode system to study the influence of the ENE on the whole cell voltage. For the HER tests, a glassy carbon electrode (5 mm diameter) drop cast with 0.2 mg_{pt} cm^{-2} 40 wt% Pt/Ketjenblack (from catalyst ink of 5 mg ml^{-1} 40 wt% Pt/Ketjenblack in IPA : deionized water : 5 wt% Nafion ionomer solution = 4 : 1 : 0.0486, to form 10 wt% Nafion ionomer in the catalyst layer), Hg/HgO (1 M KOH) electrode. And a Ni mesh (2 cm * 2 cm) were employed as the working, reference and counter electrodes, respectively.

in-situ ATR-FTIR

The in-situ ATR-FTIR tests were conducted using in our previous paper.[1] A Bruker Vertex 80 connected with an electrochemical VeeMax III apparatus from PIKE. A MCT detector with liquid nitrogen cooling was used. A Si prism evaporated with a 5 nm Ti layer and a 25 nm Au layer by an HHV 306 e-beam metal evaporator was used to reflect the signal at 60 degree angle. The catalysts were drop-casted onto the surface of the prism to form a catalyst layer of ca. 0.3 mg_{Pt} cm^{-2} 40 wt% Pt/C and used as working electrodes. An Ag/AgCl (saturated KCl) and a graphite rod were used as reference and counter electrodes, respectively. The electrolyte of 1 M KOH + 0.5 M glycerol was used. The in-situ signals under chronoamperometry tests at different potentials were captured.

in-situ Raman

The in-situ Raman tests were carried out by an i-Raman® Plus 785H Raman spectrometer with a laser wavelength of 785 nm. The catalysts were drop-casted onto a glassy carbon electrode as the working electrode (1 mg_{Pt} cm^{-2} 40 wt% Pt/C), of which the plane was set to perpendicular to the incident laser. An Ag/AgCl (saturated KCl) and a Pt wire were used as reference and counter electrodes, respectively. The anolyte and catholyte is separated by a

Nafion 212 membrane. The anolyte of 1 M KOH + 0.5 M glycerol and catholyte of 1 M KOH were used. The spectrum was acquired under chronoamperometry tests at different potentials.

MEA cell preparation

The membrane electrode assembly (MEA) electrolyzer was prepared using catalyst-coated substrate (CCS) method revised from procedures in our previous publications.[2, 3] The catalyst ink was prepared by mixing 50 mg of 40 wt% Pt/C catalyst with 15 mL isopropanol, 5 mL deionized water and 0.24 mL 10wt% FAA-3 ionomer solution (Nafion D-520 solution was used instead when acidic catholyte is used), then ultrasonicating it for at 1 hour. The anode was prepared by air spraying the anode catalyst ink onto the nickel fiber paper with a Pt loading of 3 mg/cm^2, and the cathode was prepared by air spraying the cathode catalyst ink onto carbon paper with a Pt loading of 1 mg/cm^2. The air spraying was conducted on a hot plate at 90 ^{o}C. The electrode was later dried in a vacuum oven at 80 ^{o}C overnight. The Sustainion X37-50 Grade T AEM was immersed in 1 M KOH solution for at least 24 hours to convert it to hydroxide form, washed with deionized water and used for MEA preparation in wet form. The MEA was fabricated by sandwiching cathode | AEM | anode. Stainless steel 316l blocks with a single serpentine channel were used as bipolar plates (titanium bipolar plate was used as cathodic bipolar plate when acid electrolyte was used). Viton gaskets with suitable thickness were also placed to prevent the liquid/gas from leaking. The torque applied to assemble the cell was 8.5 Nm and the active area of the MEA was 4 cm^2.

MEA cell tests

The cell temperature was maintained at 80 ^{o}C by two electric heating plates and measured by a thermocouple placed beside the two bipolar plates. The electrolyte was pumped into the cell by peristaltic pump and preheated in a heating coil before pumped into the cell. The electrochemical tests were conducted with an Autolab potentiostat with a 20-A booster (Metrohm). The I-V tests were conducted from -0.6 to 1.3 V with a scan rate of 10 mV s^{-1} to avoid serious carbon corrosion. The polarization curves were obtained by running chronopotentiometry test at various current densities for 10 min and the outlet product electrolyte was collected and later analyzed by high performance liquid chromatography (HPLC). All experiments were conducted at least three times to draw the error bars to show reliability and repeatability.

Product analysis

Chromatographic determination of glycerol oxidation products was analyzed by an Agilent 1260 Infinity II HPLC (Agilent Technologies) using the method previously reported[4]. The column used was an Aminex HPX87-H (Bio-Rad) and the eluent used was 5 mM sulfuric acid. During the test, 25 µL pre-mixed solution of 0.6 ml 0.5 M H_2SO_4 and 0.5 ml sample solution was injected into the column and the temperature of the column was kept at 60 ^{o}C. The flow rate was 0.5 mL/min. The separated compounds were then detected with a refractive index detector (RID) and a multiple wavelength detector (MWD). The expected products were also analyzed by HPLC to perform a standard calibration curve.

IC measurement

The anolyte in the sulfate crossover tests was collected and diluted for ion-chromatography (IC) measurement. The IC tests were performed by an ICS-1000 Ion Chromatography System using a Dionex IonPac AS11 with EGC III KOH as the eluent.

Density functional theory (DFT) calculations

DFT is used within the Vienna ab initio simulation package (VASP) to calculate the free energies.[5] A 3 × 3 × 1 supercell cell of Pt(111) slab with four layers (bottom two layer fixed) is constructed as substrate electrocatalysts and 4 × 4 × 1 Monkhorst−Pack k-point grids are used. The vacuum layer is larger than 15 Å to prevent the

interaction between periodical slabs. Grimme's D3 method is employed to consider the van der Waals (vdW) interactions.[6] The cut-off energy is set as 500 eV. The systems are optimized until energy and force are less than 10^{-5} eV and 0.01 eV/Å. The constant potential method is used to calculate the potential-dependent energy of the systems.[7] The VASPsol code is used to model the aqueous environment with a relative permittivity of 80.[8, 9] The effective surface tension parameter and Debye screening length are set to 0 and the 3.0 Å in VASPsol, separately. The charges for each system are added from -1.5 e to +1.5 e in steps of 0.5 e to clarify the electrode potential function. The pH effect for electrode potential is set as $U_{RHE} = U_{SHE} + k_B T ln(10) pH/e$.

Supplementary Discussion and Additional Experimental Results

Faradaic efficiency (FE) calculations

The FE of GOR product is calculated based on the following equation:

$$FE\ (\%) = \frac{nC}{Q} \times V \times F \times 100\% \quad \text{(S1)}$$

where *n* is the number of electrons transferred to produce the product, *C* is the concentration of the product (M), *V* is the volume of the electrolyte (L), *F* is the Faradaic constant (96485 C mol^{-1}), and *Q* is the total charge passed during the electrolysis (C). The value for *n* for each reaction is calculated based on the reaction pathways for glycerol oxidation in alkaline solution (Scheme S1) and listed in table S1.

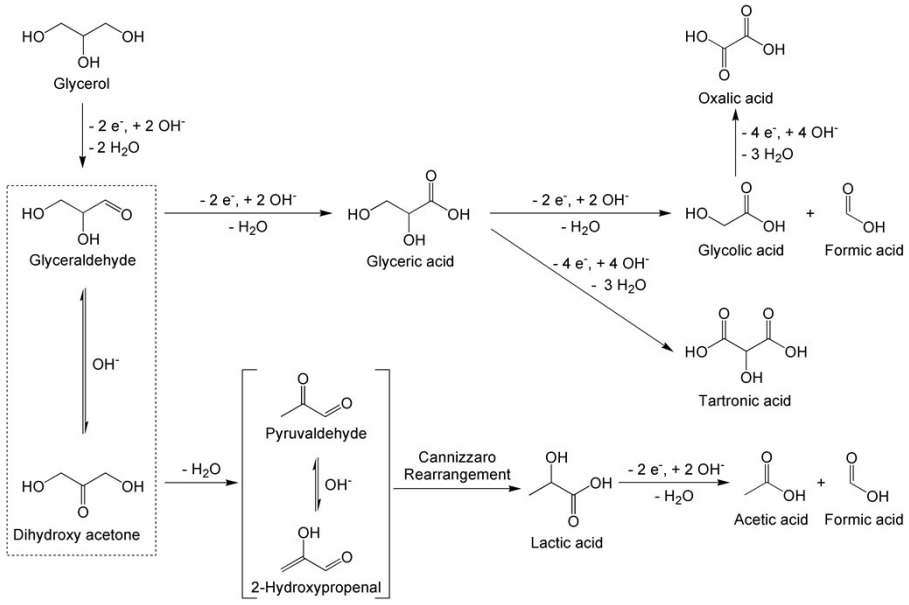

Scheme S1. Reaction pathways for glycerol oxidation in alkaline solution (reprint from reference [4]).

Table S1. The number of electron transfer for each GOR liquid product (product in salt form as GOR was conducted in alkaline electrolyte in this work)

Product	Reaction	n
Glycerate (GLA)	$CH_2OHCHOHCH_2OH + 5OH^- \rightarrow CH_2OHCHOHCOO^- + 4H_2O + 4e^-$	4
Tartronate (TA)	$CH_2OHCHOHCH_2OH + 10OH^- \rightarrow {}^-OOCCHOHCOO^- + 8H_2O + 8e^-$	8
Lactate (LA)	$CH_2OHCHOHCH_2OH + 3OH^- \rightarrow CH_3CHOHCOO^- + 3H_2O + 2e^-$	2
Glycolate (GA)	$CH_2OHCHOHCH_2OH + 6.5OH^- \rightarrow 1.5CH_2OHCOO^- + 5H_2O + 5e^-$	10/3
Acetate (AA)	$CH_2OHCHOHCH_2OH + 3.5OH^- \rightarrow 1.5CH_3COO^- + 3.5H_2O + 2e^-$	4/3
Oxalate (OA)	$CH_2OHCHOHCH_2OH + 14OH^- \rightarrow 1.5{}^-OOCCOO^- + 11H_2O + 11e^-$	22/3
Formate (FA)	$CH_2OHCHOHCH_2OH + 11OH^- \rightarrow 3\ HCOO^- + 8H_2O + 8e^-$	8/3

Energy consumption calculation for electrochemical hydrogen production

The energy to obtain hydrogen is the multiple of the charge transfer (*Q*) and the cell voltage (U_{EC}(j)). Hence, the energy consumption can be expressed as:

$$W_e = I \times U_{EC}(j) \times t = Q \times U_{EC}(j) \quad \text{(S2)}$$

where, W_e is energy consumption for hydrogen production (kWh (kg H_2)$^{-1}$) and U_{EC} is the electrochemical cell voltage (V). To produce 1 kg hydrogen, $Q = n \times F \times 1000/M_{H_2}$ ($M_{H_2}$is the molar mass of hydrogen (2 g mol^{-1})).

The equation to obtain 1 kg of hydrogen can therefore be expressed as:

$$W_e = \frac{nF}{3600 \times M_{H_2}} U_{EC}(j) = 26.8 \times U_{EC}(j) \quad \text{(S3)}$$

Calculation of the GOR standard potential

For the glycerol oxidation reaction to formic acid (take formic acid but not carbon dioxide as an example product due to the negligible FE towards carbon dioxide at lower potentials), the anode and cathode reactions can be expressed as:

Anode: $CH_2OHCHOHCH_2OH\ (l) + 5\ H_2O\ (l) \rightarrow 3\ HCOOH\ (l) + 8\ H^+ + 8\ e^-$

Cathode: $8\ H^+ + 8\ e^- \rightarrow 4\ H_2\ (g)$

Overall: $CH_2OHCHOHCH_2OH\ (l) + 3\ H_2O\ (l) \rightarrow 3\ HCOOH\ (l) + 4\ H_2\ (g)$

At 298 K and 1 atm, the Gibbs free energy can be express as:

$$\Delta G_r^0 = 3\Delta G_f^0(FA)_{liq} + 4\Delta G_f^0(H_2)_{gas} - \Delta G_f^0(GLY)_{liq} - 3\Delta G_f^0(H_2O)_{liq} = 3 * (-361.4) + 475.5 + 4 * 237.2 = 3$$
$$mol_{GLY}^{-1}$$

Considering that

$$U_{cell}^0 = \frac{\Delta G^o}{nF} \quad \text{(S4)}$$

where n is the number of electrons transferred (n = 2), and F is the Faraday constant (96485 C mol^{-1}). The standard potential for glycerol oxidation to formic acid at 298 K and 1 atm is therefore 0.0004 V. Meanwhile, the standard potential for oxygen evolution reaction (OER) is 1.229 V.

The standard potentials *vs.* SHE of OER, GOR and HER reactions at 298 K and 1 atm are:

$2\ H_2O \rightarrow O_2(g) + 4\ H^+ + 4\ e^-, E_{OER}^0 = 1.229\ V$

$CH_2OHCHOHCH_2OH\ (l) + 3\ H_2O\ (l) \rightarrow 3\ HCOOH\ (l) + 8\ H^+ + 8\ e^-, E_{GOR}^0 = 0.0004\ V$

$2\ H^+ + 2\ e^- \rightarrow H_2\ (g), E_{HER}^0 = 0\ V$

According to the Nernst equation, the thermodynamic equilibrium potentials at 298 K and 1 atm for these two reactions can be presented by Equation S3 & S4:

$$E_{OER} = E_{OER}^0 - \frac{RT}{nF} ln\left(\frac{1}{(p_{O_2}/p^0)[H^+]^4}\right) = E_{OER}^0 - 0.0148 \times lg\left(\frac{1}{p_{O_2}/p^0}\right) - 0.0592 \times pH$$

$$E_{GOR} = E_{GOR}^0 - \frac{RT}{nF} ln\left(\frac{[CH_2OHCHOHCH_2OH]}{[HCOOH]^3[H^+]^8}\right) = E_{GOR}^0 - 0.0074 \times lg\left(\frac{[CH_2OHCHOHCH_2OH]}{[HCOOH]^3}\right) - 0.0592 \times pH$$

$$E_{HER} = E_{HER}^0 - \frac{RT}{nF} ln\left(\frac{(p_{H_2}/p^0)}{[H^+]^2}\right) = E_{HER}^0 - 0.0296 \times lg\left((p_{H_2}/p^0)\right) - 0.0592 \times pH$$

where *R* is the universal gas constant, *T* is the temperature in Kelvins, *n* is the number of electrons transferred, and *F* is the Faraday constant.

Consequently, as shown in Figure S1, for the electrochemical water splitting, when pH values of anolyte and catholyte are equal, the theoretical potential 1.229 V *vs.* standard hydrogen electrode (SHE). However, if the pH values of anolyte and catholyte are 14 and 0, respectively, the theoretical potential is reduced to only 0.400 V. The same theoretical potential reduction assisted by ENE can also be applied to the GOR-coupled HER, as the glycerol oxidation reaction is also a proton-coupled electron transfer reaction, and the reduced cell voltage can be up to 829 mV theoretically. The potential for GOR to formic acid *vs.* SHE reduces from 0.0004 V at pH 14 to -0.8284 V at pH 0. This makes the onset cell voltage reduce from 0.0004 to -0.8284 V. Besides, the negative onset cell voltage allows the cogeneration of electricity and hydrogen.

In addition, according to the Nernst equation, there is a positive relationship between the ENE and temperature. Therefore, the reduction in the cell voltage via ENE harvesting is theoretically more significant at higher temperatures.

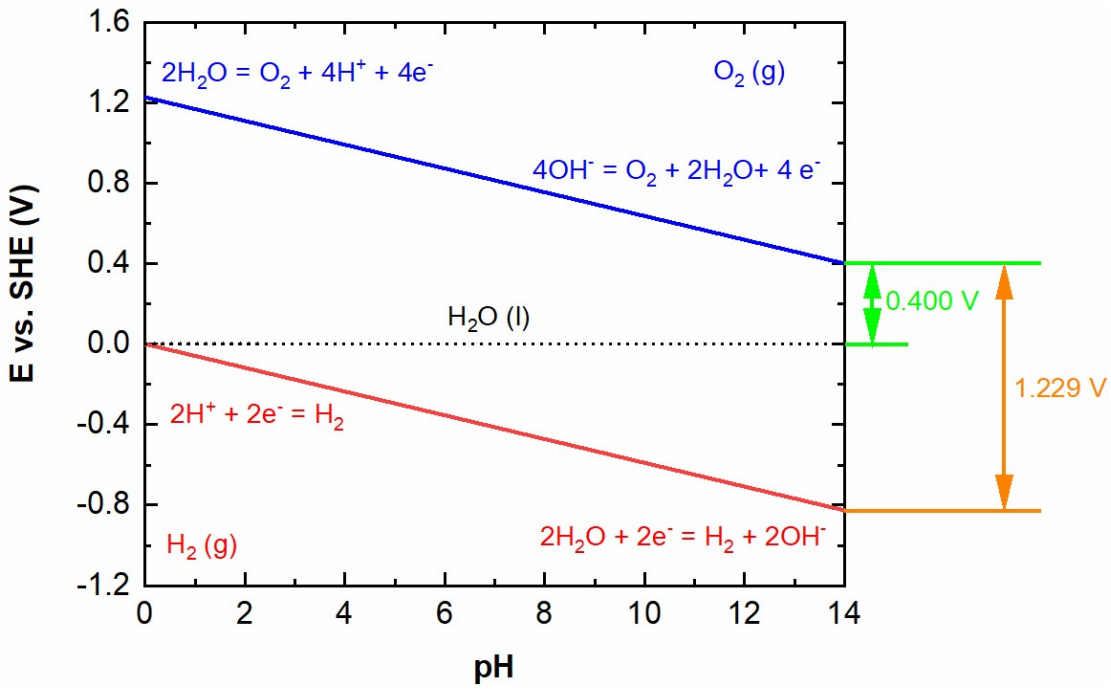

Figure S1. The Pourbaix diagram of water calculated by the Nernst equation showing the theoretical potentials for the OER, GOR and HER.

Mass transport in the MEA electrolyzer

The current density, j_i, depends on the flux of the species *i*:

$$j_i = -nFJ_i \quad \text{(S5)}$$

where $J_i(x)$ is the flux of species i at distance x from surface (mol s^{-1} cm^{-2}). The mass transport in the MEA electrolyzer is composed of diffusion, migration and convection. The total flux can be expressed by the Nernst-Planck equation:

$$J_i(x) = -D_i\frac{\partial C_i(x)}{\partial x} - \frac{Z_iF}{RT}D_iC_i\frac{\partial \emptyset(x)}{\partial x} + C_iv(x) \quad \text{(S6)}$$

where D_i is the diffusion coefficient ($cm^2\ s^{-1}$), $\frac{\partial C_i(x)}{\partial x}$ is the concentration gradient along distance x, Z_i and C_i are the charge (dimensionless) and concentration (mol cm^{-3}) of species i, $\frac{\partial \emptyset(x)}{\partial x}$ is the potential gradient along distrance x, $v(x)$ is the velocity profile of the solution. (Red: diffusion; blue: migration; green: convection).

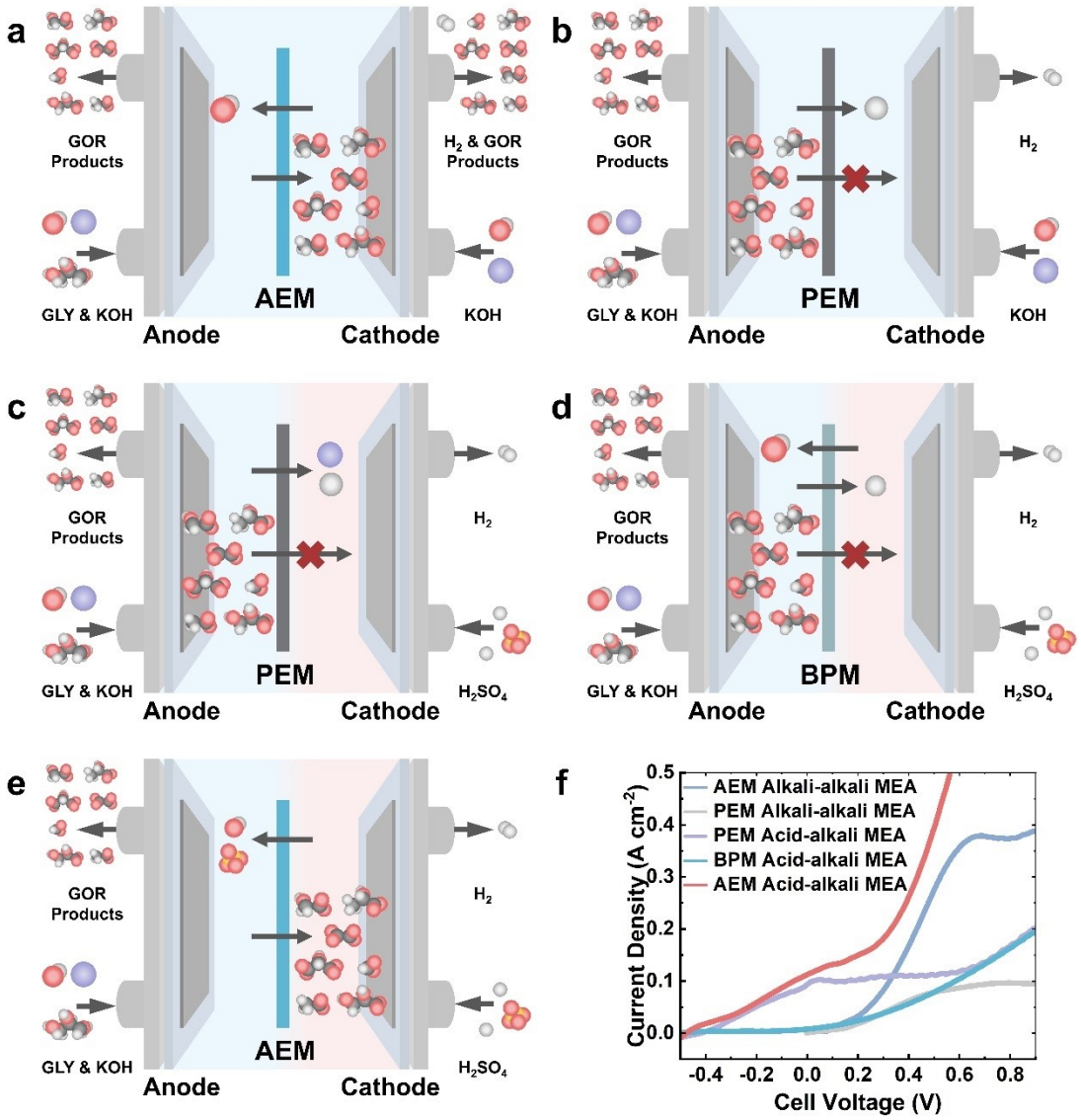

Figure S2. MEA configurations and descriptions for GOR-coupled HER. Graphical schematics of (a) AEM-based alkali-alkali, (b) PEM-based alkali-alkali, (c) PEM-based acid-alkali, (d) BPM-based acid-alkali, (e) AEM-based acid-alkali MEA devices, and (f) the corresponding GOR I-V curves.

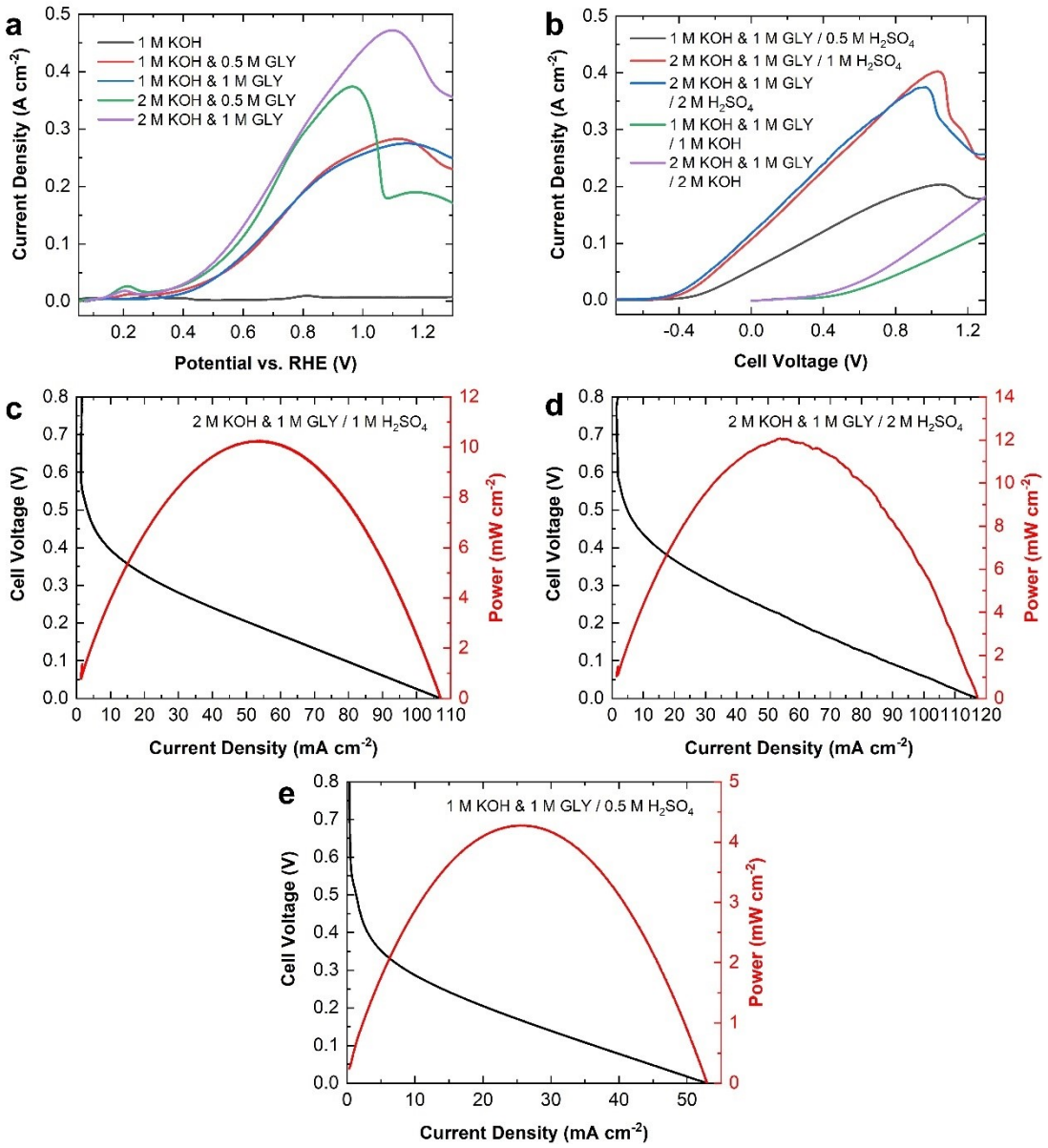

Figure S3. (a) LSV curves of GOR on Pt/C in alkaline electrolyte with or without various glycerol concentrations in an H-cell measured by a three-electrode system; (b) I-V curves of GOR on Pt/C in an alkali-alkali and acid-alkali H-cell with various electrolyte concentrations measured by a two-electrode system; (c-e) cell performance as an electricity generator with polarization and power density curves of acid-alkali H-cell with various electrolyte concentrations (both at room temperature and 80 °C).

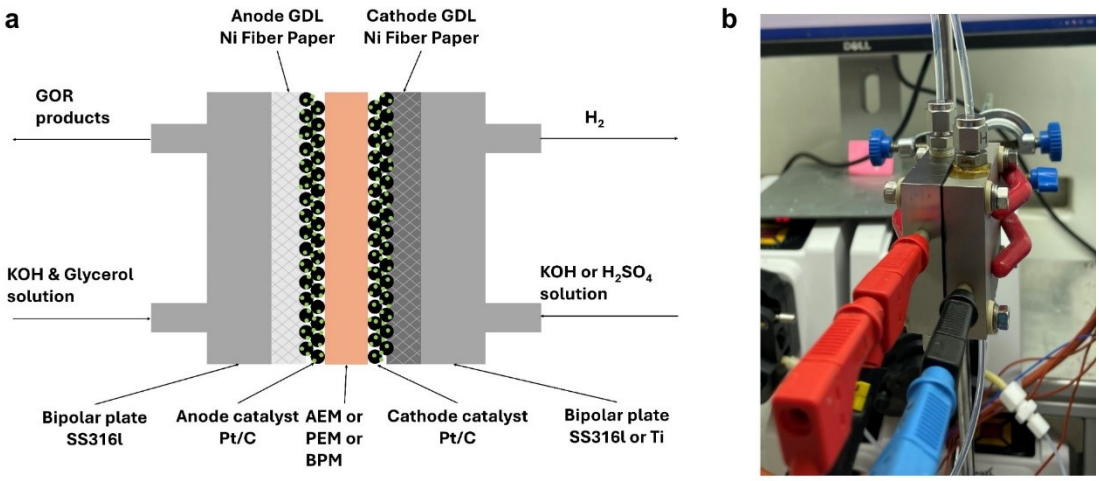

Figure S4. (a) Cross-sectional schematic illustration of the MEA electrolyzer for GOR and hydrogen production used in this work. When AEM or PEM is used, only anion or cation is allowed to cross the membrane. When the BPM is used, the water is dissociated into proton and hydroxide catalyzed by TiO_2, and the proton and hydroxide then enter the cathode and anode through CEM and AEM, respectively. (b) A photo of the MEA electrolyzer for GOR and hydrogen production.

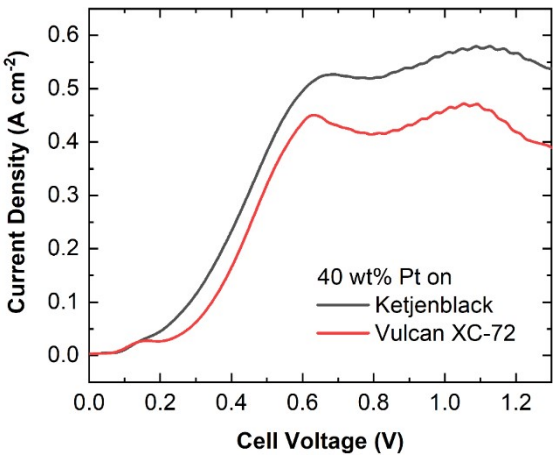

Figure S5. I-V curves of GOR in 1 M KOH & 1 M glycerol with a flow rate of 5 ml min^{-1} at 80 °C, catalyzed by 40 wt% Pt on high surface area Ketjenblack and on Vulcan XC-72. The 40 wt% Pt on Ketjenblack shows higher GOR activity, and it was therefore used for the tests in this work.

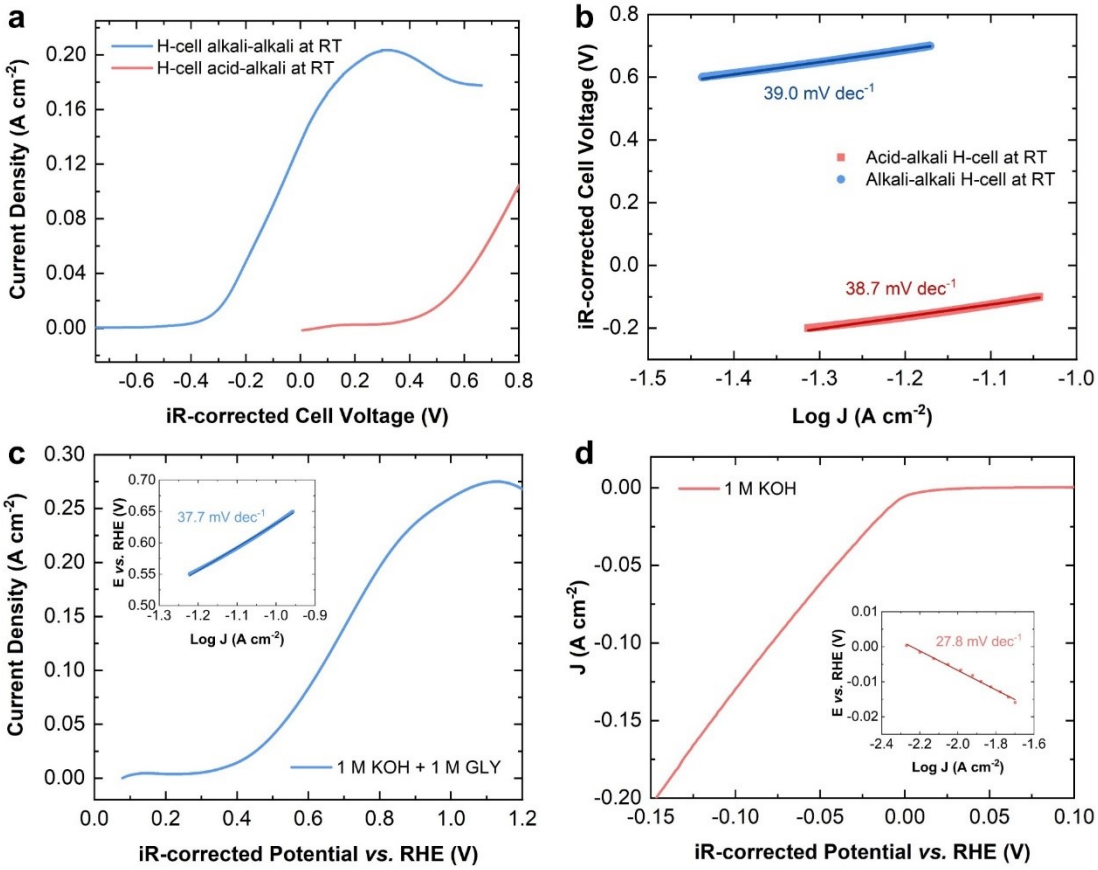

Figure S6. (a) I-V curves and (b) corresponding Tafel curves of GOR in 1 M KOH & 1 M glycerol anolyte with 1 M KOH / 0.5 M $H2SO_4$ catholyte at RT measured by two-electrode system in an H-cell. The LSV curves and the corresponding Tafel plots of (c) GOR in 1 M KOH & 1 M glycerol and (d) HER in 1 M KOH measured by three-electrode system in an H-cell (85% system resistance used for iR compensation).

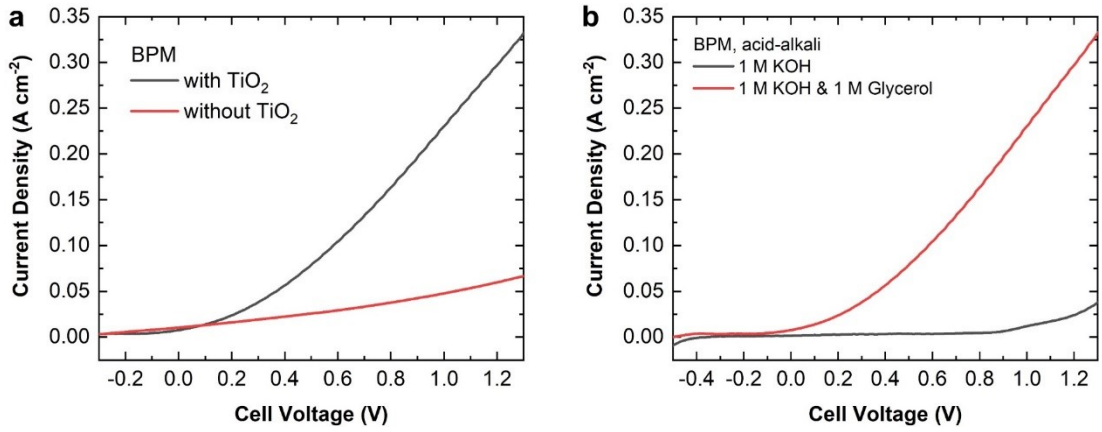

Figure S7. (a) I-V curves of GOR in 1 M KOH & 1 M glycerol (0.5 M H_2SO_4 to cathode) with a flow rate of 5 ml min^{-1} at 80 °C, using BPM with or without TiO_2 in between the CEM and AEM. The BPM without TiO_2 was prepared simply by assembling the Sustainion X37-50 AEM and Nafion 212 CEM in wet form directly after immersed in deionized water for at least one hour. The BPM with TiO_2 preparation was adapted from literatures[10, 11]. The Nafion 212 was air sprayed with 30 μg cm^{-2} TiO_2 (anatase, 25 nm) before assembled with Sustainino X37-50 and the TiO2 is in the middle and served as the water dissociation catalyst. It can be found from the figure that the TiO_2 water dissociation catalyst enhances the GOR activity significantly. (b) I-V curves of GOR in 1 M KOH & 1 M glycerol anolyte in a BPM-based acid-alkali dual MEA electrolyzer at 80 °C.

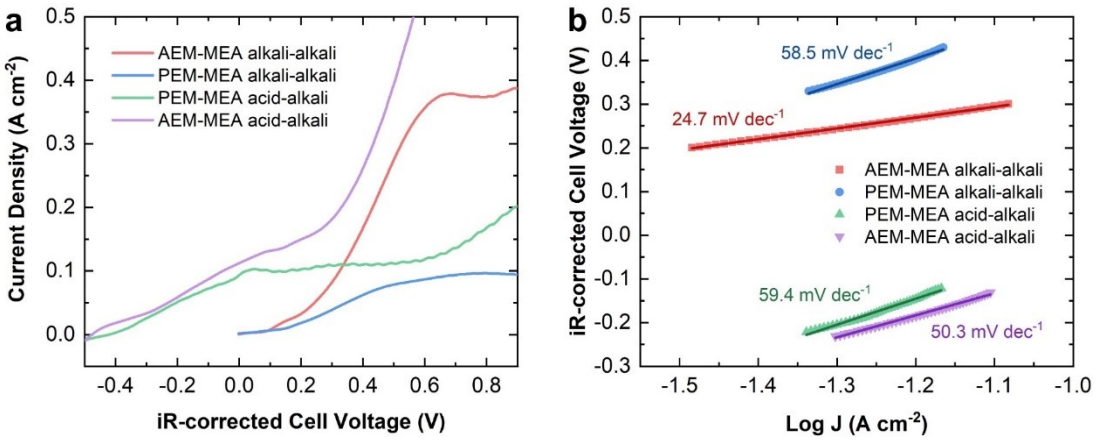

Figure S8. (a) I-V curves and (b) corresponding Tafel curves of GOR in 1 M KOH & 1 M glycerol anolyte with 1 M KOH / 0.5 M $H2SO_4$ catholyte in AEM- and PEM-based MEA reformers at 80 °C.

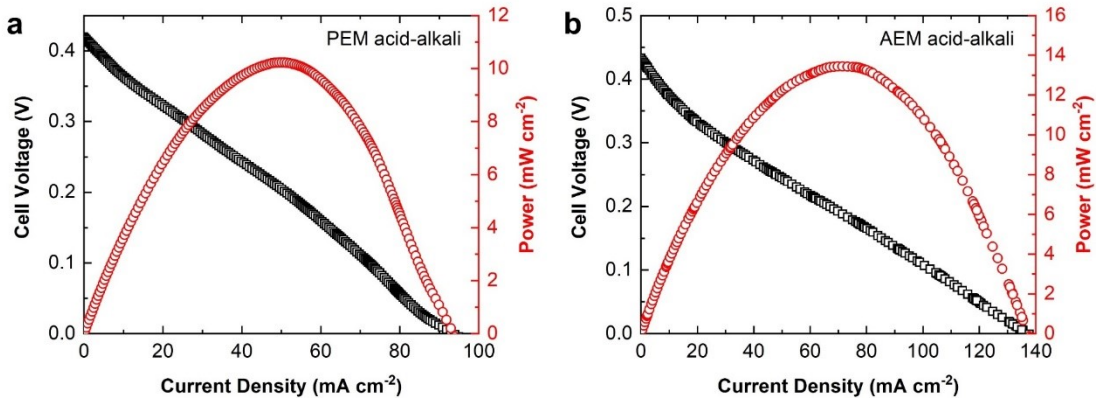

Figure S9. Cell performance as an electricity generator with polarization curve and power density curve in (a) PEM-based and (b) AEM-based acid-alkali MEA electrolyzer at 80 °C.

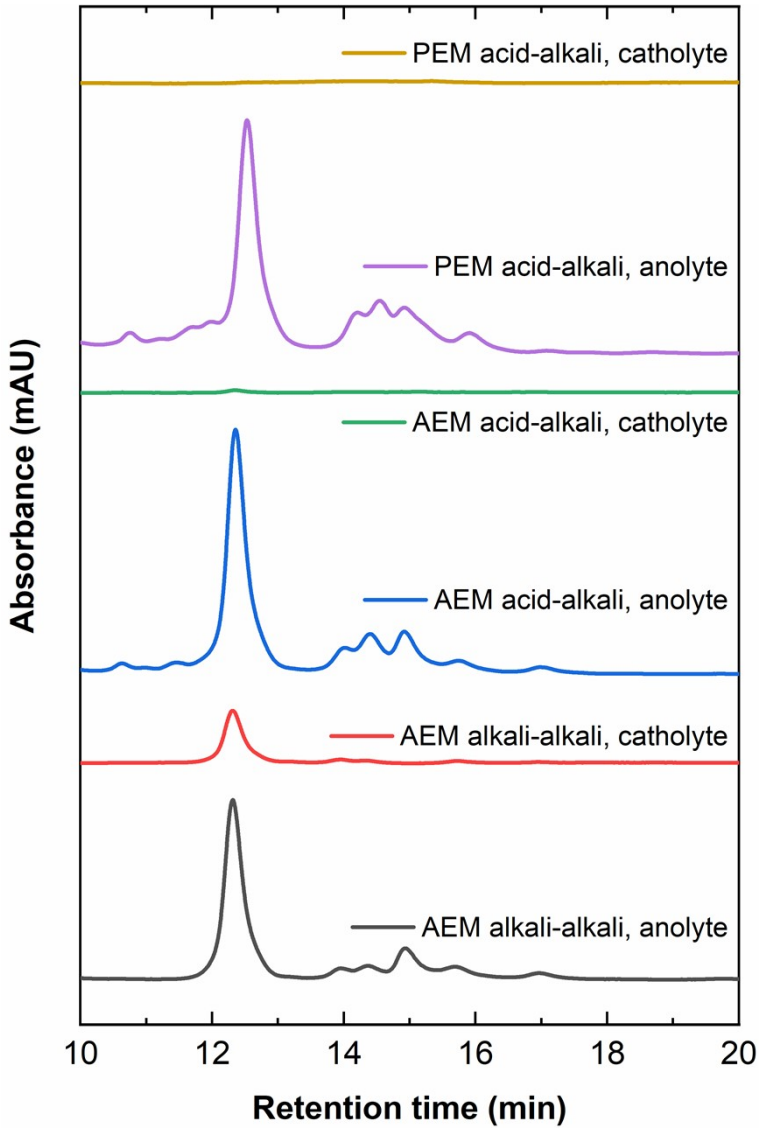

Figure S10. HPLC curves of catholyte and anolyte of GOR (1 M KOH & 1 M GOR anolyte, 1 M KOH or 0.5 M H_2SO_4 pumped into the cell at 5 ml min^{-1} at 80 °C) in AEM alkali-alkali, AEM acid-alkali, and PEM acid-alkali cells. It can be observed from the figure that the liquid crossover is obvious in the AEM alkali-alkali cell, and minimal in AEM acid-alkali cell, and negligible in PEM acid-alkali cell.

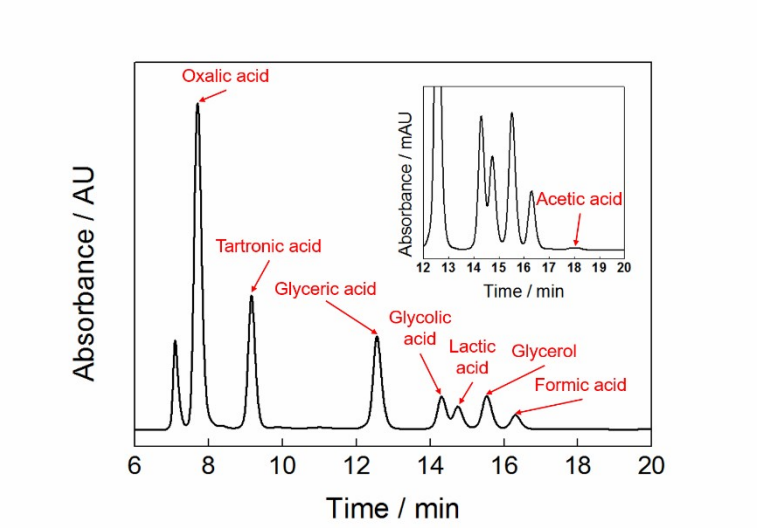

Figure S11. The assignment of each peak to GOR products in the HPLC (reprint from Ref. 1).

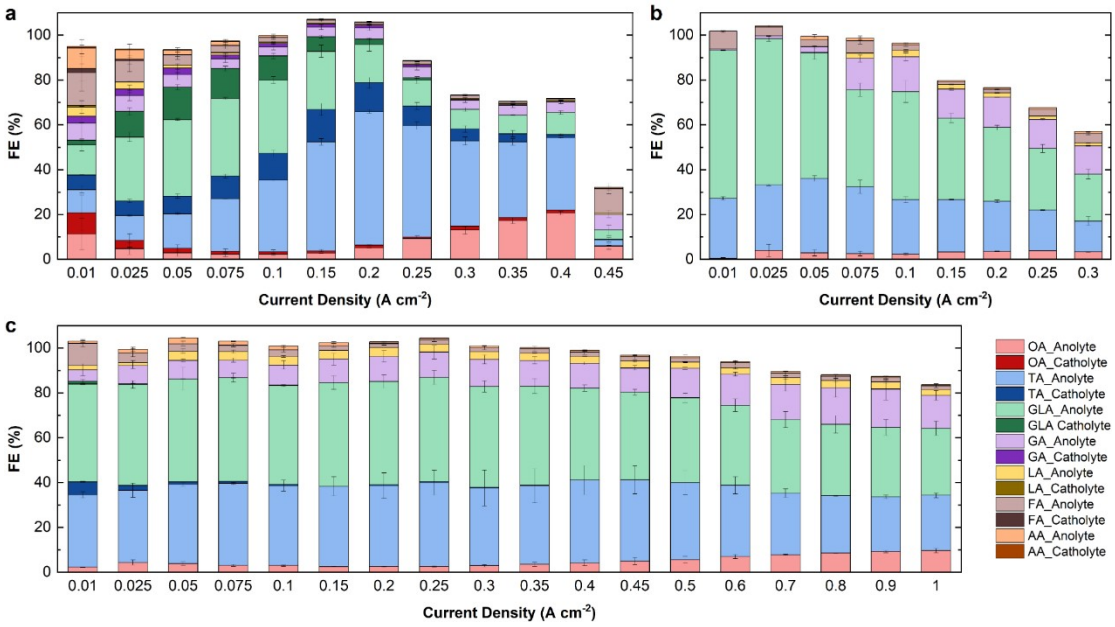

Figure S12. FE of each GOR product in (a) AEM-based alkaline-alkaline, (b) PEM-based acid-alkaline, and (c) AEM-based acid-alkaline MEA electrozlyers with 1 M KOH & 1 M glycerol anolyte pumped at 5 ml min^{-1} at 80 ^{o}C. (OA: oxalate; TA: tartronate; GLA: glycerate; GA: glycolate; LA: lactate; FA: formate; AA: acetate)

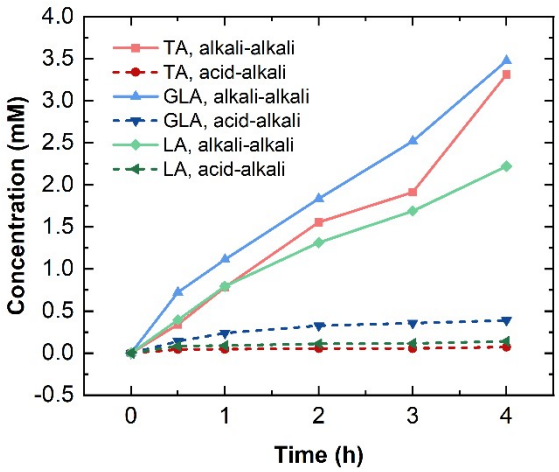

Figure S13. Concentrations of C3 (TA, GLA and LA) crossed from anolyte to catholyte at open circuit voltage (OCV) with time in AEM-based alkali-alkali and acid-alkali MEA electrolyzers with 1 M KOH & 1 M glycerol & 0.1 M potassium tartronate & 0.1 M potassium glycerate & 0.1 M potassium lactate anolyte and 1 M KOH / 0.5 M H_2SO_4 catholyte pumped at 5 ml min^{-1} at 80 ^oC. The volume of anolyte/catholyte was 50 ml, and the electrolytes were pumped and cycled to measure the effect of increased anolyte catholyte pH difference on the product anion crossover rate to support the hypothesis that increased hydroxide crossover rate can suppress the product anion crossover.

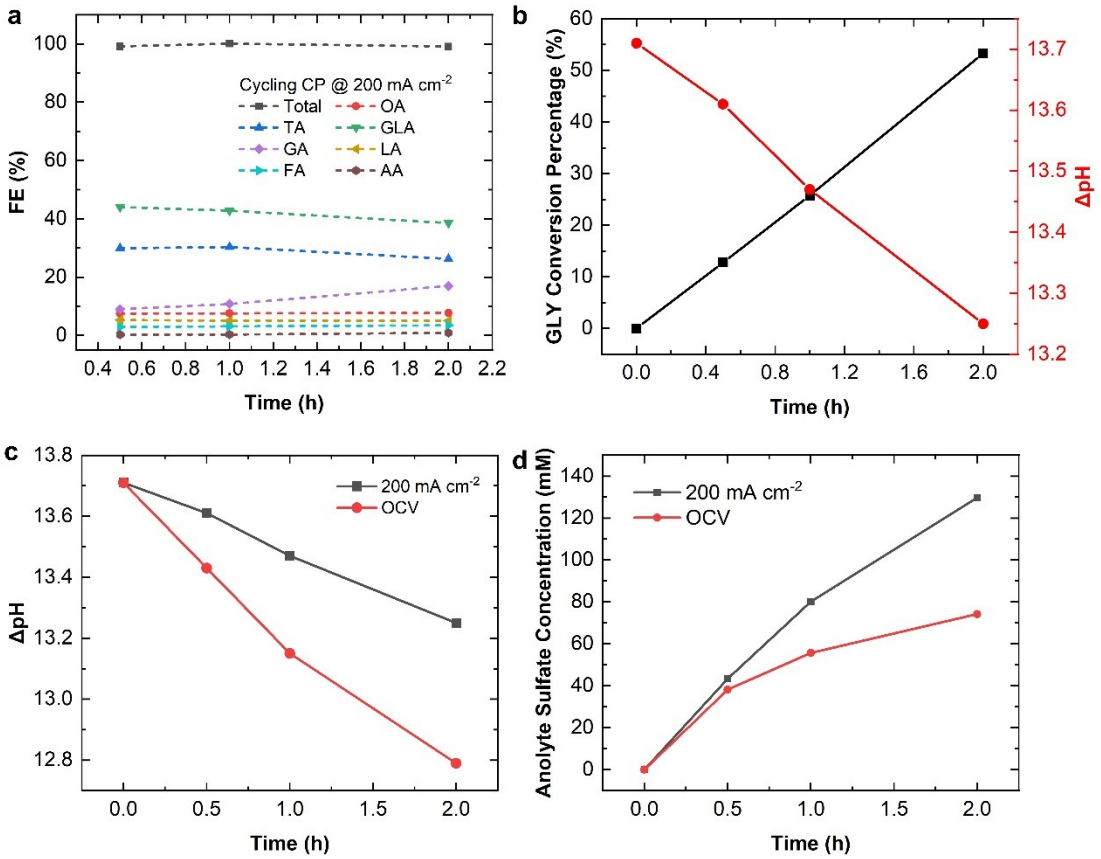

Figure S14. Stability of the (a) product FEs at current densities of 200 mA cm^{-2}, (b) the change of glycerol conversion ratio and pH difference between anolyte and catholyte with time, (c) the change of pH difference between anolyte and catholyte, and (d) sulfate concentration in anolyte via crossover under OCV and 200 mA cm^{-2}, with time of AEM-based acid-alkali MEA electrolyzer with 1 M KOH & 0.5 M glycerol anolyte and 0.5 M H_2SO_4 catholyte pumped at 5 ml min^{-1} at 80 °C. The volume of anolyte/catholyte was 50 ml, and the electrolytes were pumped and cycled to measure the change in product selectivity, pH and activity with consumption of glycerol.

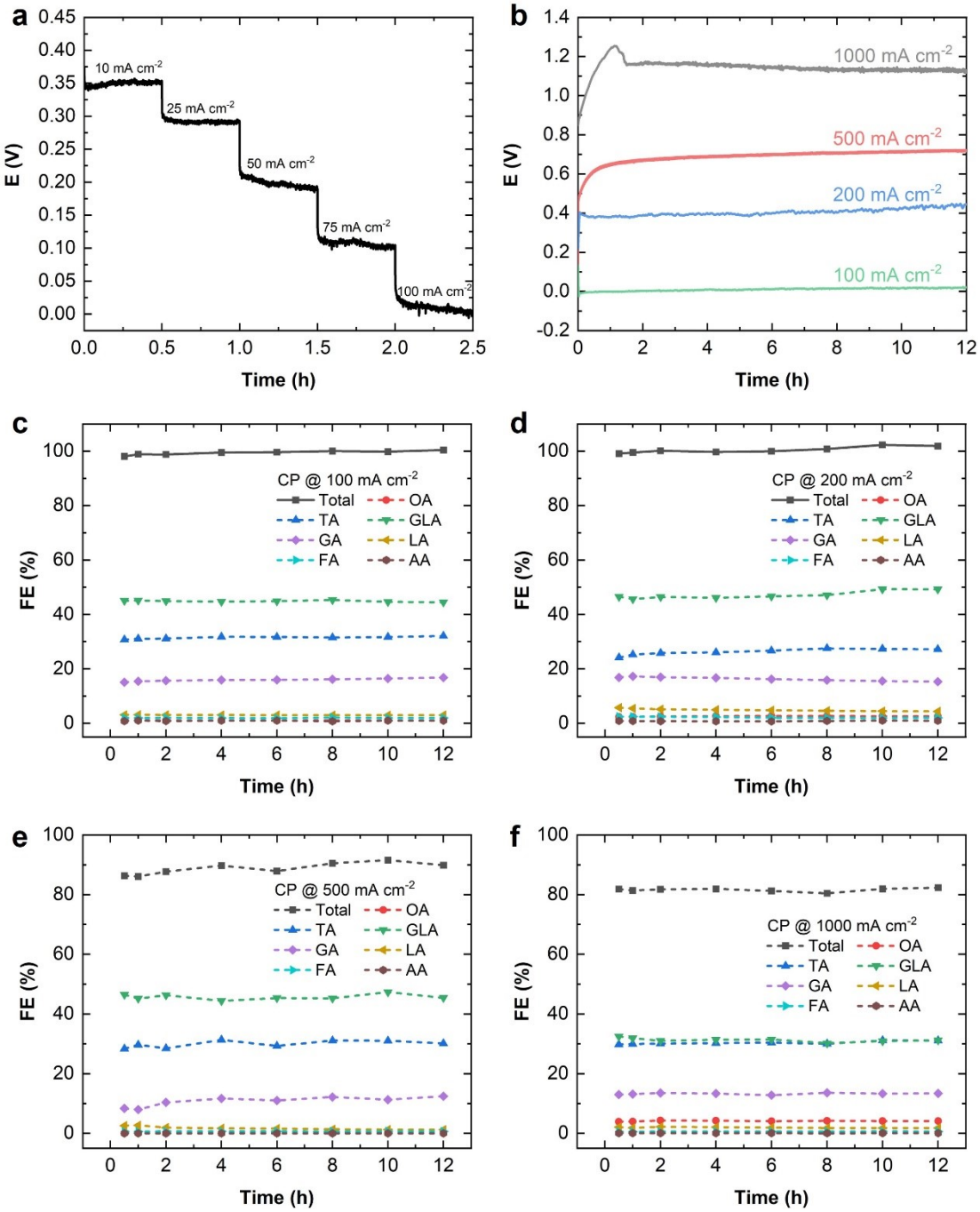

Figure S15. (a) Stability of the AEM-based acid-alkali MEA electrolyzer as a hydrogen production electricity generator with 1 M KOH & 1 M glycerol anolyte and 0.5 M H_2SO_4 catholyte pumped at 5 ml min^{-1} at 80 ^oC at various current densities; (b) stability of the AEM-based acid-alkali MEA electrolyzer with 1 M KOH & 1 M glycerol anolyte and 0.5 M H_2SO_4 catholyte pumped at 5 ml min^{-1} at 80 ^oC at current densities of 100, 200, 500 and 1000 mA cm^{-2}, and (c-f) the corresponding faradaic efficiencies (FEs) towards various liquid products and the total values.

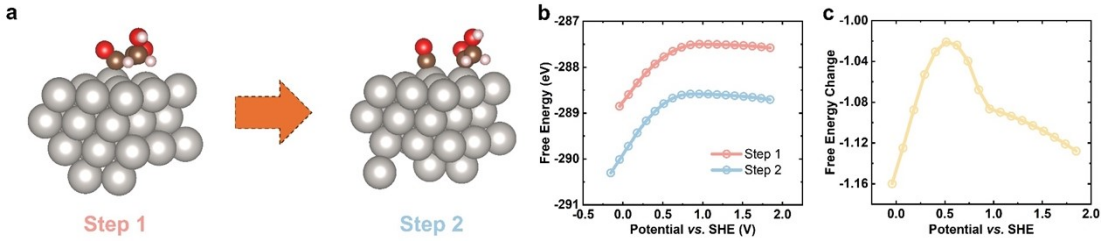

Figure S16. (a) The optimized adsorption geometry of species before and after C-C bond cleavage on Pt (111) surface ($CH_2OHC^*OC^*O_{ads} \rightarrow CH_2OHC^*O_{ads} + CO_{ads}$), and the corresponding (b) free energy values of step 1 & 2, and (c) the free energy changes at various potentials *vs.* SHE.

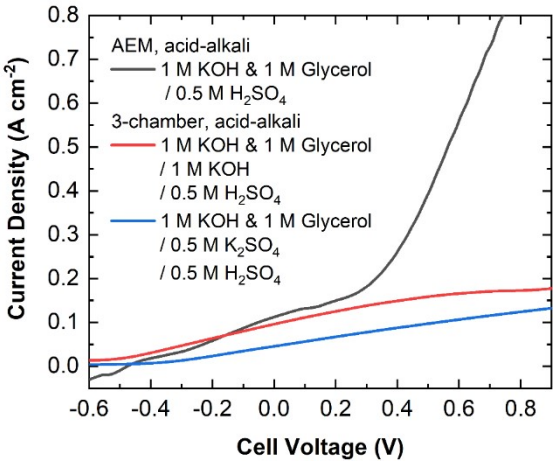

Figure S17. Comparison of GOR in acid-alkali devices with and without an extra chamber flown with 1 M KOH or 0.5 M K_2SO_4 electrolyte. The extra chamber, made of PEEK, placed between the AEM on the anode side and PEM on the cathode side, is pumped with electrolyte at 5 ml min^{-1}. In such 3-chamber device, the performance is better using 1 M KOH as electrolyte in the extra chamber. This is because the more sufficient supply of hydroxide ion from the extra chamber to anode via AEM. However, the AEM-based acid-alkali MEA system outperforms significantly at larger current densities, as a result of the greatly increased system resistance from the extra chamber.

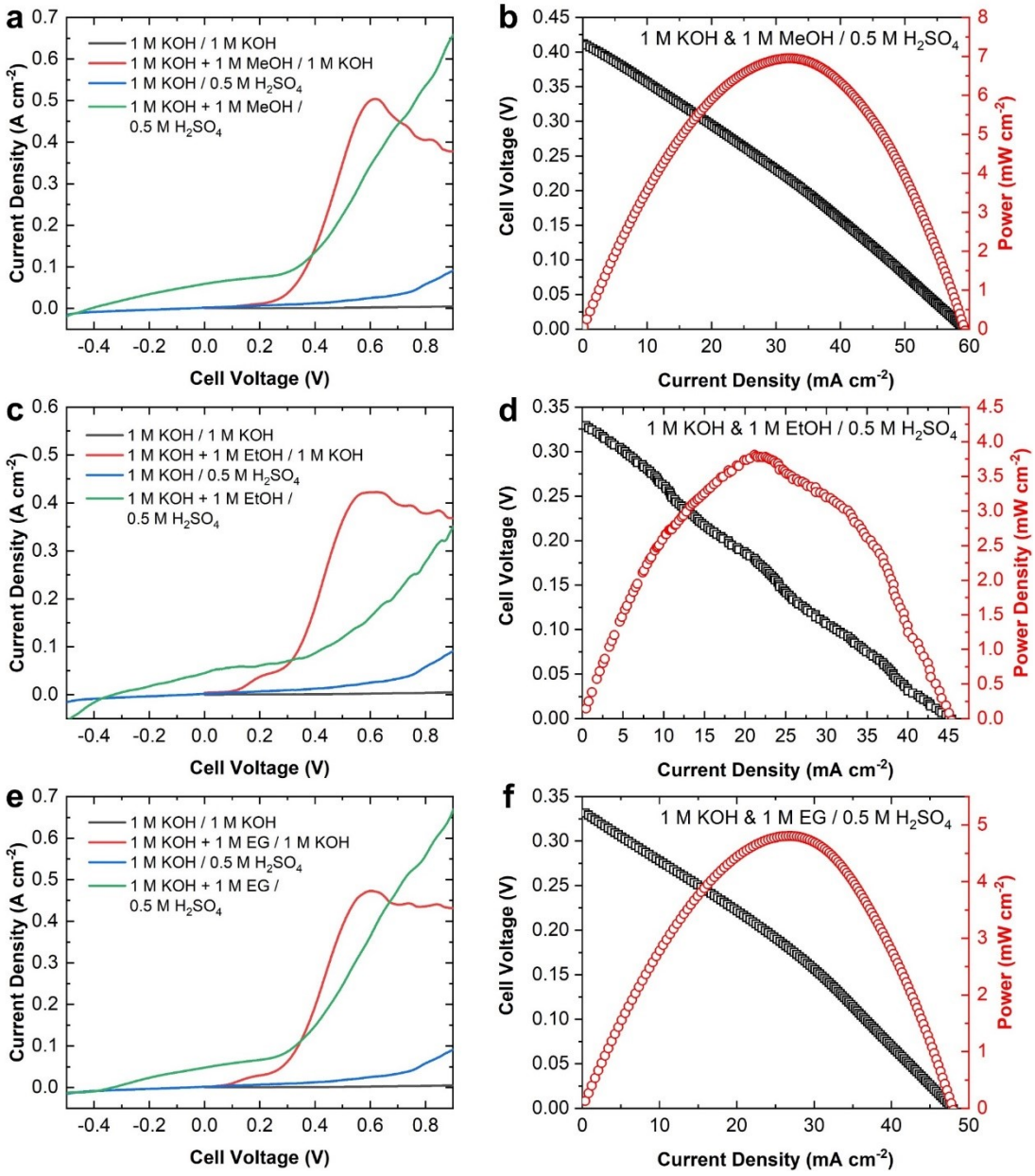

Figure S18. (a, c, e) I-V curves of electrochemical oxidation of methanol (MeOH), ethanol (EtOH) and ethylene glycol (EG) in alkali-alkali and acid-alkali MEA electrolyzers, and (b, d, e) cell performance as a electricity generator with polarization and power density curves of acid-alkali MEA electrolyzers using MeOH, EtOH and EG as fuels, at 80 °C. These results prove the versatile applications of the acid-alkali MEA electrolyzer on simultaneous hydrogen and electricity generation with valorization of other organic substances.

Table S2. A comparison of hydrogen production from small molecule anodization in alkaline coupling the HER in acid to harvest ENE.

Anode reactant	Anode catalyst	Electrolyte	Membrane	Performance	Ref.
HzOR[a]	$Ni_{0.5}Co_{0.5}Se_2$/CC[b]	1 M KOH & Hydrazine[c] / 0.5 M H_2SO_4	BPM	Fuel cell power density of 13.3 mW cm^{-2} at a current density of 54.7 mA cm^{-2}	[12]
Urea	CuCl/rGO[d]	2 M KOH & 0.5 M Urea / 0.5 M H_2SO_4	BPM	Cell voltage of 0.83 V to achieve 10 mA cm^{-2} in LSV	[13]
Glucose	$Fe_{0.1}$-$CoSe_2$/CC	1 M KOH & 0.5 M glucose / 0.5 M H_2SO_4	BPM	Cell voltage of 0.72 V to achieve 10 mA cm^{-2} in LSV	[14]
Glycerol	Cu–Cu_2O/CC	1 M KOH & 0.5 M glycerol / 0.5 M H_2SO_4	BPM	Cell voltage of 0.59 V to achieve 10 mA cm^{-2} in LSV	[15]
Glycerol	CoNiCuMnMo/CC	1 M KOH & 0.1 M glycerol / 0.5 M H_2SO_4	CEM	Cell voltage of 0.55, 0.89 and 1.25 V to achieve 10, 100 and 200 mA cm^{-2} in LSV	[16]
Phenylcarbinol	NiO-NSs/NF[e]	1 M KOH & 50 mM phenylcarbinol / 0.5 M H_2SO_4	BPM	Cell voltage of 0.686 V to achieve 10 mA cm^{-2} in chronopotentiometry	[17]
Glycerol	**Pt/C**	**1 M KOH & 0.5 M glycerol / 0.5 M H_2SO_4**	**AEM**	**Cell voltage of -0.361, 0 and 0.377 V to achieve 10, 100 and 200 mA cm^{-2} in chronopotentiometry.**	**This work**

a. Hydrazine oxidation reaction (HzOR); b. carbon cloth (CC); c. hydrazine concentration not mentioned; d. reduced graphene oxide (rGO); e. NiO nanosheets supported on Ni foam (NiO-NSs/NF).

Table S3. Performance of GOR-coupled hydrogen production in a two-electrode system.

Anode catalyst	Cathode catalyst	Cell	Membrane	T (°C)	Anolyte	Catholyte	$U_{EC, LSV}$ [a]	FE	Ref
NiO / NF [b]	NiMoNH / NF	MEA[c]	Fumasep FAB-PK-130	RT[d]	1 M KOH & 0.1 M GLY	1 M KOH	1.54 V @ 100 mA cm^{-2}	NA	18
CoNiCuMnMo / CC [e]	RhIr / Ti	Flow cell	CEM [f]	RT	1 M KOH & 0.1 M GLY	1 M KOH	1.34, 1.66 V @ 10, 100 mA cm^{-2}	NA	16
						0.5 M H_2SO_4	0.55, 0.89 V @ 10, 100 mA cm^{-2}	92% to formate @ 50 mA cm^{-2}	
Cu–Cu_2O/CC	Pt/C	H-cell	BPM	RT	1 M KOH & 0.5 M GLY	0.5 M H_2SO_4	0.59 V @ 10 mA cm^{-2}	93.5% to formate @ 10 mA cm^{-2}	15
NC/Ni–Mo–N/NF	NC/ Ni–Mo–N/NF	Single cell	None	RT	1 M KOH & 0.1 M GLY		1.38 V @ 10 mA cm^{-2}	NA	19
Ni–Mo–N/CFC [g]	Ni–Mo–N/CFC	Single cell	None	RT	1 M KOH & 0.1 M GLY		1.35 V @ 10 mA cm^{-2}	95.0% towards formate @ 1.4 V	20
PtRu/C	Pt/C	MEA	KOH-doped PBI [h]	75	4 M KOH & 2 M GLY	2 M KOH	0.48 V @ 0.1 A cm^{-2}	NA	21
Pd/TNTA [i]	Pt/C	MEA	Tokuyama A201	80	2 M NaOH & 2 M GLY	2 M NaOH	0.33, 0.52, 0.62 V @ 0.1, 0.2, 0.5 A cm^{-2}	NA	22
NiCo hydroxide	Pt mesh	H-cell	Nafion 117	RT	1 M KOH & 0.1 M GLY	1 M KOH	1.35 & 1.59 V @ 0.01, 0.1 A cm^{-2}	94.3% towards formate @ 100 mA cm^{-2}	23
Pt/C	**Pt/C**	**MEA**	**Sustainion X37-50**	**80**	**1 M KOH & 0.5 M GLY**	**1 M KOH**	**0.14, 0.28, 0.37, 0.60 @ 0.01, 0.1, 0.2, 0.5 A cm^{-2}**	**$FE_{liq,total}$ [j] close to 100% @ J up to 0.2 A cm^{-2}**	**This work**
						0.5 M H_2SO_4	**-0.44, -0.06, 0.33, 0.56 @ 0.1, 0.2, 0.5 A cm^{-2}**	**$FE_{liq,total}$ close to 100 @ J up to 0.4 A cm^{-2}. 95.9% and 83.5% @ 0.5 and 1 A cm^{-2}**	

a. $U_{EC, LSV}$: whole-cell voltage obtained from LSV curves; b. NF: Nickel foam; c. MEA: membrane electrode assembly electrolyzer; d. RT: room temperature; e. CC: carbon cloth; f. CEM: cation exchange membrane; g. CFC: carbon fiber cloth; h. PBI: polybenzimidazole; i. TNTA: 3D nanostructured TiO_2 nanotube arrays; j. $FE_{liq,total}$: total of FEs towards all liquid products.

Table S4. Molar selectivity towards C3 products from GOR in alkaline media.

Anode catalyst	Cathode catalyst	System	T (°C)	Anolyte	Catholyte	Molar selectivity towards C3 product	Ref.
Pt@G[a]	Graphite	3-E[b]	RT	1 M KOH & 20 mM GLY	1 M KOH	ca. 90%, 85%, 80% and 60% @ 2.4, 4.3 11.3 and 15.7 mA cm^{-2} (PV[c]@0.6, 0.7, 1.0 & 1.1 V *vs.* RHE)	[24]
PtRhNi/GNS[d]	Pt gauze	3-E	RT	0.5 M KOH & 0.5 M GLY	0.5 M KOH	54.2% and 42.5% @ 1.8 and 1.6 mA cm^{-2} (CA[e]@-0.1 and 0.2 V *vs.* SCE)	[25]
Pt/CNTs[f]-CeO_2	Pt wire	3-E	50	1 M KOH & 0.1 M GLY	1 M KOH	ca. 90% @ 7 mA cm^{-2} (CA@0.8 V *vs.* RHE)	[26]
Ag/Pd sheet	Pt plate	3-E	RT	1 M KOH & 0.1 M GLY	1 M KOH	34.1% @ 22 mA cm^{-2} (CA@-0.1 V *vs.* Hg/HgO)	[27]
Pt-CeO_2/CNT	Pt wire	3-E	60	1 M KOH & 0.1 M GLY	1 M KOH	95% @ 34 mA cm^{-2} (CA@0.9 V *vs.* RHE)	[28]
PdAg/CNT	Acta 4020	AEM-DGFC[g]	60	4 M KOH + 1 M GLY	O_2	43.2% @ 17.9 mA cm^{-2} (CA@0.1 V)	[29]
ALD(TiO_2)-Au/C	Pt wire	3-E	60	0.1 M KOH + 0.1 M GLY	0.1 M KOH	76.1 @ 4 mA cm^{-2} (0.7 V *vs.* Hg/HgO)	[30]
Au-P4P/G[h]	Pt foil	3-E	RT	0.5 M NaOH + 0.5 M GLY	0.5 M NaOH	82% & 60% @ 12.3 & 26 mA cm^{-2} (CA@0.2 & 0.6 V vs. Hg/HgO)	[31]
AuPt (15% Pt_{surf})	Graphite rod	3-E	RT	1 M KOH & 0.5 M GLY	1 M KOH	89.3%, 87.9%, 87.4% and 52.3% @ 2.5, 14.2, 36.7 and 61.2 mA cm^{-2} (CA@0.45, 0.6, 0.9 and 1.05 V *vs.* RHE)	[4]
Pt/C	**Pt/C**	2-E	**80**	**1 M KOH & 0.5 M GLY**	**0.5 M H_2SO_4**	**88.0%, 84.2%, 82.2%, 81.8%, 76.3% and 70.2% @10, 50, 100, 200, 500 and 1000 mA cm^{-2}**	**This work**

a. Pt@G: graphitic Pt nanocrystal; b. 3-E: three-electrode system; c. PV: pulse voltammetry; d. GNS: graphene nanosheet; e. CA: chronoamperometry; f. CNTs: carbon nanotubes; g. AEM-DGFC: anion exchange membrane direct glycerol fuel cell; h. Au-P4P/G: Au-poly(4-vinylpyridine)/graphene.

Table S5. Prices of reactants and possible value-added products of electrochemical glycerol oxidation reaction[32-36]

Chemical	Industrial Price ($ per t)	Production (Mt/yr)
Glycerol	500 (crude) – 1,000 (purified)	4.3
Glycolic acid	1,840 – 2,800	0.04
Oxalic acid	1,200 – 1,400	0.19
Formic acid	800 – 1,080	0.95
Glyceraldehyde	2,110	0.35
Dihydroxyacetone	2,000 – 3,800	0.33
Acetic acid	680 – 920	10
Lactic acid	1,580 – 1,870	0.45
Glyceric acid	2,300 – 2,800	NA
Tartronic acid	4,670	NA

Table S6. A comparison of cell potentials (U_{EC}) obtained from chronopotentiometry tests at 0.1 & 0.2 A cm^{-2} and the corresponding energy consumption (W_e) of hydrogen production coupling with alkaline OER, GOR and GOR with ENE in an MEA electrolyzer at 80 °C.

Methods	Catalyst	Electrolyte	U_{EC} @ 0.1 & 0.2 A cm^{-2} (V)	W_e @ 0.1 & 0.2 A cm^{-2} (kWh / kg H_2)	Ref.
Alkaline OER	$Ni_{0.56}Fe_{0.44}OOH$	1 M KOH	1.42 & 1.44	38.1 & 38.6	[37]
GOR	40 wt% Pt/C	1 M KOH	0.361 & 0.491	9.65 & 13.1	This work
GOR with ENE	40 wt% Pt/C	1 M KOH / 0.5 M H_2SO_4	0 & 0.377	0 & 10.2	This work

Table S7. Electricity cost for hydrogen production via various methods (data used in **Table S5**).

Methods	W_e @ 0.1 & 0.2 A cm^{-2} (kWh / kg H_2)	Electricity Cost (USD / kg H_2)[a]
Alkaline OER	38.1 & 38.6	2.95 & 2.99
GOR	9.65 & 13.1	0.748 & 1.02
GOR with ENE	0 & 10.2	0 & 0.791

a. Price calculated based on the average industrial electricity cost in US. The average industrial electricity prices are 7.75, 9.3 and 22.31 US cents per kWh in US, China and Singapore, respectively

References

1. L. B. Sun, C. C. Dai, T. J. Wang, X. D. Jin, Z. J. Xu and X. Wang, *Angew Chem Int Edit*, 2024, **63**.
2. F. Meng, C. Dai, Z. Liu, S. Luo, J. Ge, Y. Duan, G. Chen, C. Wei, R. R. Chen, J. Wang, D. Mandler and Z. Xu, *eScience*, 2022, **2**, 87-94.
3. S. Luo, C. Dai, Y. Ye, Q. Wu, J. Wang, X. Li, S. Xi and Z. J. Xu, *Angew Chem Int Ed Engl*, 2024, DOI: 10.1002/anie.202402184, e202402184.
4. C. Dai, L. Sun, H. Liao, B. Khezri, R. D. Webster, A. C. Fisher and Z. J. Xu, *J. Catal.*, 2017, **356**, 14-21.
5. G. Kresse and J. Furthmuller, *Phys Rev B Condens Matter*, 1996, **54**, 11169-11186.
6. S. Grimme, *J Comput Chem*, 2006, **27**, 1787-1799.
7. Q. Wu, C. C. Dai, F. X. Meng, Y. Jiao and Z. J. Xu, *Nature Communications*, 2024, **15**.
8. K. Mathew, R. Sundararaman, K. Letchworth-Weaver, T. A. Arias and R. G. Hennig, *J Chem Phys*, 2014, **140**, 084106.
9. M. Fishman, H. L. Zhuang, K. Mathew, W. Dirschka and R. G. Hennig, *Physical Review B*, 2013, **87**, 245402.
10. L. Chen, Q. Xu, S. Z. Eoner, K. Fabrizio and S. W. Boettcher, *Nature Communications*, 2022, **13**, 3846.
11. B. Siritanaratkul, P. K. Sharma, E. H. Yu and A. J. Cowan, *Advanced Materials Interfaces*, 2023, **10**, 2300203.
12. G. Wang, J. Chen, P. Cai, J. Jia and Z. Wen, *J Mater Chem A*, 2018, **6**, 17763-17770.
13. G. Wang, J. Chen, Y. Li, J. Jingchun, P. Cai and Z. Wen, *Chemical Communications*, 2018, **54**, 2603-2606.
14. D. Zheng, J. Li, S. Ci, P. Cai, Y. Ding, M. Zhang and Z. Wen, *Applied Catalysis B: Environmental*, 2020, **277**, 119178.
15. B. Liu, G. Wang, X. Feng, L. Dai, Z. Wen and S. Ci, *Nanoscale*, 2022, **14**, 12841-12848.
16. L. Fan, Y. Ji, G. Wang, J. Chen, K. Chen, X. Liu and Z. Wen, *Journal of American Chemical Society*, 2022, **144**, 7224-7235.
17. C. Zhang, S. Ci, X. Peng, J. Huang, P. Cai, Y. Ding and Z. Wen, *J Energy Chem*, 2021, **54**, 30-35.
18. S. Li, D. Liu, G. Wang, P. Ma, X. Wang, J. Wang and R. Ma, *Nano-Micro Lett*, 2023, **15**, 189.
19. Y. Xu, M. Liu, S. Wang, K. Ren, M. Wang, Z. Wang, X. Li, L. Wang and H. Wang, *Applied Catalysis B: Environmental*, 2021, **298**, 120493.
20. Y. Li, X. Wei, L. Chen, J. Shi and M. He, *Nature Communications*, 2019, **10**, 5335.
21. J. d. Paula, D. Nascimento and J. J. Linares, *Journal of Applied Electrochemistry*, 2015, **45**, 689-700.
22. Y. X. Chen, A. Lavacchi, H. A. Miller, M. Bevilacqua, J. Filippi, M. Innocenti, A. Marchionni, W. Oberhauser, L. Wang and F. Vizza, *Nature Communications*, 2014, **5**, 4036.
23. Z. Y. He, J. W. Hwang, Z. H. Gong, M. Z. Zhou, N. A. Zhang, X. W. Kang, J. W. Han and Y. Chen, *Nature Communications*, 2022, **13**.
24. W. Chen, L. Zhang, L. Xu, Y. He, H. Pang, S. Wang and Y. Zou, *Nat Commun*, 2024, **15**, 2420.
25. Y. F. Zhou, Y. Shen and J. H. Piao, *Chemelectrochem*, 2018, **5**, 1636-1643.
26. X. S. Liu and C. C. Yang, *Mater Lett*, 2022, **324**.
27. H. Inoue, S. Kimura, Y. Teraoka, M. Chiku, E. Higuchi and B. T. X. Lam, *Int J Hydrogen Energ*, 2018, **43**, 18664-18671.
28. J. F. Li, Z. Y. Li, Z. X. Zheng, X. Q. Zhang, H. Zhang, H. Wei and H. B. Chu, *Chemcatchem*, 2022, **14**.
29. N. Benipal, J. Qi, Q. Liu and W. Z. Li, *Appl Catal B-Environ*, 2017, **210**, 121-130.
30. J. Han, Y. Kim, D. H. K. Jackson, K. E. Jeong, H. J. Chae, K. Y. Lee and H. J. Kim, *Electrochem Commun*, 2018, **96**, 16-21.

31. H. Wang, L. Thia, N. Li, X. Ge, Z. Liu and X. Wang, *Applied Catalysis B: Environmental*, 2015, **166-167**, 25-31.
32. E. A. Moges, C.-Y. Chang, M.-C. Tsai, W.-N. Su and B. J. Hwang, *EES Catalysis*, 2023, **1**, 413-433.
33. Á. Vass, B. Endrodi and C. Janáky, *Current Opinion in Electrochemistry*, 2021, **25**, 100621.
34. K.-E. Guima, L. M. Alencar, G. C. da Silva, M. A. G. Trindade and C. A. Martins, *ACS Sustainable Chemistry & Engineering*, 2018, **6**, 1202-1207.
35. H. J. Kim, Y. Kim, D. Lee, J.-R. Kim, H.-J. Chae, S.-Y. Jeong, B.-S. Kim, J. Lee, G. W. Huber, J. Byun, S. Kim and J. Han, *ACS Sustainable Chemistry & Engineering*, 2017, **5**, 6626-6634.
36. M. Braun, C. S. Santana, A. C. Garcia and C. Andronescu, *Current Opinion in Green and Sustainable Chemistry*, 2023, **41**, 100829.
37. J. E. Park, S. Park, M.-J. Kim, H. Shin, S. Y. Kang, Y.-H. Cho and Y.-E. Sun, *ACS Catalysis*, 2022, **12**, 135-145.